In-situ Observation of the Soot Deposition Process on a Solid Wall with a Diffusion Flame along the Wall

Jae-Hyuk CHOI*

Osamu FUJITA**

Takahumi TSUIKI***

Junhong KIM****

Suk-Ho CHUNG*****

Key Words: Diffusion combustion, Boiler, Flame, Soot, Deposition, Volume fraction, Microgravity, Soot line

* Division of Mechanical Science, Hokkaido University,
Kita13, Nishi8, Kita-ku, Sapporo, 060-8628, Japan
E-mail: jhhair@york-me.eng.hokudai.ac.jp

**Division of Mechanical Science, Hokkaido University
E-mail: ofujita@eng.hokudai.ac.jp

***Mitsubishi Heavy Industries, LTD
Higashi-Tanaka, Komaki, Aichi, 485-8561, Japan
E-mail: sakigake0812@hotmail.com

****School of Mechanical and Aerospace Engineering
Seoul National University, Seoul, 151-742, Korea
E-mail: junhk75@snu.ac.kr

***** School of Mechanical and Aerospace Engineering
E-mail: shchung@snu.ac.kr

Abstract

Experiments at the Japan Microgravity Center (JAMIC) have investigated the interaction between diffusion flames and solid surfaces placed near flames. The fuel for the flames was C_2H_4 and the surrounding oxygen concentration 35%, with surrounding air temperatures of T_a=300 and 600K. The effects of these parameters on soot distribution in diffusion flames and soot deposition on solid walls were studied. Direct images of the whole flame and shadow images of the flame with back light were recorded and used to calculate the soot volume fraction by the Abel transformation method. Results show that at the higher surrounding air temperature the soot particle distribution region is closer to the wall and results in more deposition. Numerical simulation was also performed to determine the motion of soot particles in the flames and the soot deposition characteristics. The results are in good agreement with the observed soot behavior in microgravity.

1. Introduction

Soot particles play an important role as a heat radiation medium for heat exchangers in boilers and chemical reactors, while it is one of the most common air pollutants and soot deposition to walls may cause hot spots in internal combustion engines. Consequently, the soot particle formation mechanism is an important subject for study in the combustion field. Soot formation characteristics in hot preheated air are an especially important subject when utilizing preheated air combustion in industry, but it is not well investigated. The phenomena involved in soot deposition may be studied through the adhesion process of fine particles near the surface of walls with a temperature gradient. For particle adhesion to a wall with a temperature gradient, it is known that the flow field of the gas and the thermophoretic effect near the surface of a wall are dominating factors. Rosner et al.[(1)] investigated the simultaneous action of inertial and thermophoretic effects on particle deposition in curved laminar boundary layer flows. Walker et al.[(2)] studied thermophoretically enhanced deposition, and in the analysis there the transport equation in laminar tube flow takes both diffusion and thermophoresis into account. Adomeit et al.[(3)] performed experiments and numerical simulations of deposition of fine particles from turbulent liquid flow and suggested that thermophoresis enhances the deposition on cooled surfaces, especially at low adhesion probabilities. Thakurta et al.[(4)] presented a direct numerical simulation(DNS) results for the deposition rates of TiO_2 particles on walls in turbulent channel flow with thermophoretic effects. Compared to DNS without thermophoresis, the deposition rates with thermophoresis show dramatic increases in particle deposition. Tsai et al.[(5)] examined thermophoretic deposition in external flows between parallel plate ducts with temperature gradients and developed a simple correlation to describe the thermophoretic effect on particle deposition on cold plates. Lin et al.[(6)] in a numerical used the critical trajectory method investigation of the effect of developing flows in a circular tube on the thermophoretic particle deposition efficiency. It was found that when both flow and temperature are developing, the deposition efficiency is significantly higher than in fully developed flows. However, with soot generated by actual flames this kind of research is very limited, because actual flames are strongly influenced by natural convection, and it is difficult to maintain a stable relative position between

wall surface and flame. Considering the thermophoretic effect acting on actual soot, Dobashi et al. showed that the thermophoretic force is given by the primary particle size [7)~(9)], but did not use hot soot particles present in flames but cold soot obtained after sampling. There is some research investigating the amount of soot deposition to solid media inserted in a diffusion flame [(10)(11)] that has tried to determine the amount of soot deposition in relation to the thermophoretic effect. However, this research is different from research to observe the in-situ process of soot deposition from a diffusion flame to a wall, which is the aim of the present research.

The purpose of this study was to make in-situ observations of the soot particle deposition process within a diffusion flame near a solid wall, and then to establish the details and magnitude of the thermophoretic effect on soot particles present in the flame zone. This type of investigation is important to evaluate the soot deposition in heat exchanger tubes in boiler furnaces and steam reformers where flames are present near the tubes. The experimental configuration in the investigation is chosen to be applicable to evaluating soot deposition on heat exchangers. The solid wall temperature beside the flame was heated to simulate an actual wall. In the research, a stable diffusion flame along a solid wall was formed in a microgravity environment attained at the Japan Microgravity Center (JAMIC), and the behavior of the soot adhering to the wall within the flame was observed. Numerical simulations were also performed to further elucidate details of the velocity field and temperature.

2. Experimental

2.1 Experimental setup

A schematic outline of the test burner is shown in Fig.1. The burner has dimensions of ϕ 30× 210(L)mm with a porous 20mm wide fuel exit of sintered metal, marked as porous burner in the figure. A cylindrical burner was used to eliminate edge effects that arise with boundary layer type diffusion flames with flat burners. The edge effects result in uncertainties in determining the soot distribution by the laser

extinction method. Ethylene(C_2H_4) with a mean injection velocity of U_f=0.8cm/s was used as the fuel. An electrical heater is inserted inside the cylindrical burner, and the wall temperature of the burner can be set to a given temperature (T_w=800K in the present paper). The surrounding gas($O_2$35%,N_2 balance) with a velocity V_a=5cm/s (reduced to ordinary temperature) was supplied to the combustion duct. In the experiment, the reasons for selecting T_w=800K and O_2=35% are in consideration of the temperature of the reaction tubes of actual combustion systems such as steam reformer tubes and to obtain sufficient soot formation in the flame.

Figure 2 is a schematic outline of the experimental setup. The experimental setup has a combustion duct, an imaging system, an air and fuel supply system, and a sequence controlling system, which are installed on an optical base plate for obtaining flame images. The combustion duct has inner dimensions of 130(W)×255(L)×85(H) mm, and is connected to an electric heater filled with ceramic heat accumulator to supply uniformly preheated air. The front and rear panels of the combustion duct contain Pyrex glass windows openings with dimensions of 160×49mm and 120×49mm, respectively, to allow optical access and backlight for the flame imaging system. Laser extinction images with backlight were taken with a digital video(DV) camera from the front. The top of the duct also has a pyrex window to enable recording of direct flame pictures. As the burner is cylindrical, the phenomena recorded are axisymmetric and the direct and shadow images are comparable. A 532nm wavelength laser diode was used as backlight after passing an appropriate interference filter. The laser extinction method was adopted to measure the distribution of the soot volume fraction in the laminar diffusion flame. This method depends on the mathematical inversion of path-integrated extinction data to give the radial distribution of the attenuation ratio, and hence the soot volume fraction distribution in the viewed area. The extinction profile ($\ln(I/I_0)$ with I_0 the initial intensity and I the transmitted light intensity) is inverted by Abel transformation to give the attenuation ratio as a function of the radial position in the flame, k(r). In calculating the soot volume fraction from the attenuation ratio it is assumed that soot particles are much smaller than the wavelength of the laser light($\pi D/\lambda \ll 1$: D the particle parameter and λ the laser wavelength), and that the soot particles are spherical. Under these assumptions the absorption coefficient is given by Rayleigh theory. To investigate the effect of the

surrounding air temperatures on the soot deposition on the burner wall, the surrounding air temperature was increased by an electric heater connected to the combustion duct. The microgravity environment was provided at the Japan Microgravity Center (JAMIC), which provides up to 10 seconds of high quality (less than $10^{-5}g_0$, g_0 the gravity at sea level) microgravity time.

3. Experimental Results and Discussion

First the effect of gravity on the flame behavior was investigated. Figure 3 shows a comparison of the laminar diffusion flames along a solid wall in normal gravity(a) and microgravity(b); The experimental conditions were ethylene fuel injected with a 0.8cm/s,U_f, mean fuel velocity, external airflow 5 cm/s, V_a, and 35% O_2 with N_2 balance. The surrounding air temperature and the wall temperature are 300K. In the figure, the solid arrows show the fuel exit and the dashed arrow is the direction of gravity.

In normal gravity the flame surrounding the cylindrical burner fluctuates periodically because of buoyancy and the relative position of flame and solid surface changes with time. Acceleration of the flow field may occur here and made a definition of the external flow condition impossible. In microgravity, a stable flame appears even with the very low external airflow velocity as seen in Fig.3 (b). Except for the time right after ignition, the flame shape is almost constant and maintains its position relative to the wall during the microgravity period. This situation is very desirable when attempting to observe the soot distribution within the flame. This result suggests that the use of a microgravity environment is essential to establish the interaction between flame and solid wall in determining the soot distribution. The authors believe that the presence of buoyancy-induced disturbances is the main reason why in-situ observation of the soot deposition from a diffusion flame to a wall was not possible.

Figure 4 shows direct flame photos and laser extinction images at T_a=300K and 600K under the microgravity environment. The direct flame picture is to the left and the extinction image is to the right. The extinction image shows only the top half of the flame because of the limitations of the collimated laser light width, showing the bottom horizontal black part corresponding to the burner wall. In the tests, the wall

temperature was 800K, which simulates the heated wall of the heat exchanger as is commonly seen the case for the reaction tubes of steam reformers. The air-flow was set at 5cm/s reduced to the ordinal temperature, i.e, the same mass flow rate for both 300K and 600K. According to the observations, the flame luminosity increases greatly with the higher surrounding air temperature. The visible flame position shows a tendency to approach the wall with the higher surrounding temperature. The soot distribution according to the laser extinction image showed large differences in the position of strong soot concentrations in the flame. The soot particle distribution region at 300K is clearly away from the surface of the wall in the viewed area, while at T_a=600K it approaches and finally downstream adheres to the wall. According to the extinction image, the soot concentration at T_a=600K appears to be stronger than that at T_a=300K. As explained above, it was impossible to observe such a stable soot distribution in normal gravity, while particle depositions without flames have been observed. The results shown here are the first ever to show the in-situ soot deposition process to a wall in a flame burning along a solid wall.

Figure 5 shows the flame position (“flame line” in the figure, given by the outer edge of the visible flame) in the direct image and the position of the “soot line”, defined as the position of the strongest soot concentration below the visible flame. When the surrounding air temperature is 600K the position of the visible flame is much closer to the wall than that at 300K and the soot line has also moved greatly in the direction of the wall. The large changes in the flame position with increasing surrounding air temperature are considered to be due to increases in the diffusion coefficient of the surrounding air and increases in the volumetric velocity. Particularly, the increased volumetric velocity made the fuel stream approach nearer to the wall at the higher surrounding air temperature. Hence, the stoichiometric position of the diffusion flame shifts towards the burner wall and the soot line is also closer to the wall. An interesting feature of the figure is the difference in the position of the flame and soot lines. This difference suggests that the maximum soot formation position is very far from the visible flame position in a stable laminar diffusion flame attained in microgravity. Another noteworthy feature is the behavior of the rear of the soot line at different air temperatures. The soot line with T_a=600K is convex and finally reaches the wall surface, while the T_a=300K line approaches to the wall linearly with increasing flow distance.

Figure 6 shows the trace appearance of the deposited soot taken after the experiments, and there is more soot deposition with the high temperature, corresponding to the observations in Figs. 4 and 5. In Fig. 6(a), there is soot deposition very near the fuel injection this is due to adhesion before the start of the drop, not deposition in microgravity. When the surrounding air temperature is 600K, soot adheres about 70-80mm from the front end of the fuel injection.

Figure 7 shows the soot volume fraction distribution determined from the laser extinction image in Fig.4 with the 300K and 600K surrounding air temperatures. The figure shows the distribution of soot in the direction normal to the external flow at different distances from point of gas injection (z=50,70,90, and 110mm; with z defined as the distance from the front of the sintered metal fuel exit). The results show that the soot concentration at 600K is much higher than that at 300K, and that with the higher air temperature, the soot distribution moves to the burner wall at all observed positions as pointed out in the description of the extinction images. For example, the position of maximum concentration at z=70mm is 6mm from the wall at 600K, and 10mm at 300K; at z=110mm, the position is 3mm at 600K and 7mm at 300K. Another notable feature is that the maximum concentration tends to increase with increases in z. This implies that the widely distributed soot between flame and wall concentrates towards one position at a given z. An explanation of the soot distribution change along the z direction is shown in Fig.8, here soot is formed under the flame and is moved in the wall direction under the effect of gas convective motion and thermophoretic effects acting on the soot particles. There is a steep temperature gradient between flame and wall and the thermophoretic effect here is significant. Soot particles are subjected to the thermophoretic force from the high temperature region of the flame zone to the low-temperature region of the wall surface, and this force increases with the temperature gradient. The soot particle motion is, of course, also affected by the flow field above the burner, including the fuel jet and the effect of gas expansion in the combustion zone. As a result, the distribution of soot particles is determined by the balance between the effects of the thermophoretic force and convective motion.

4. Numerical Simulation

The experimental results show that with increasing surrounding air temperatures the distribution of the soot concentration generated in a flame moves closer to the surface of the wall and that it becomes easier for soot to adhere to the wall. It is surmised that the distribution of soot particles changes due to variations in the velocity field and in the temperature field by the changes in the air temperature. A numerical analysis was conducted to better understand the behavior of the laminar diffusion flame near a solid wall based on the physical model in Fig.8.

Time-dependent, axisymmetric equations in cylindrical coordinates were solved for the momentum, species, and energy equations. The calculations were based on direct numerical simulation(DNS) code with a low Mach number approximation[12], so that the zero-order pressure term is constant over the computational domain and the first-order term is governed by the Poisson equation. A finite difference procedure on a staggered grid was adopted using a second-order central difference scheme. The second-order predictor-corrector scheme used a time integration algorithm[13]. A uniform grid system was applied. The Poisson equation could not be directly solved with the spectral method, and instead the multigrid method was used in the axial direction as a fast iterative method. In the radial direction, the Poisson solver adapted the tridiagonal matrix solver (TDMA). A one-step overall reaction was adopted. This may ~~a~~ limit a detailed explanation of the flame structure; however the hydrodynamic and thermal fields can be reasonably well described. In the radial and horizontal directions, the computational dimensions were a $128 * 512$ mesh with mesh sizes of 0.31 and 0.29mm, respectively. The time step was 5μs and thermodynamic pressure constant. The profile of the fuel exit velocity is modeled as a 2-D Poiseuille flow. A uniform velocity profile was assumed for the inlet condition of the air. At the outlet, all scalar variables and velocity vectors were evaluated from the convective boundary conditions[12]. At the side wall, zero fluxes of the scalar variables and normal velocities were applied. Thermodynamic and transport properties were evaluated with CHEMKIN-Ⅲ and the Transport Package[14][15].

4.1 Numerical results and thermophoretic effects

Figure 9 shows the distribution of the temperature and V-velocity (velocity in the z direction) for the flame in Fig.4 (T_a=300,600K,T_w=800K). In this calculation, the surrounding air velocity (reduced to ordinal temperature) and fuel jet velocity were V_a=5cm/s and U_f=0.8cm/s. The wall temperature was assumed to be T_w=800K. In Fig.9, the solid and dotted lines are the flame and soot lines in Fig.5. The contours of the temperature distribution in Fig.9 are in good agreement with the observed flame shape. Comparing with Fig.5, the flame line given by the outer edge of the visible flame corresponds to a position slightly inside the maximum temperature position in Fig.9. This seems reasonable because the visible flame is the result of incandescent soot to appear on the fuel rich side rather than at the stoichiometric position, i.e, at the maximum temperature position. Figure 9 also shows that the temperature contour at T_a=600K shifts closer to the wall than in the case at T_a=300K. The V-velocity, accelerates with the z direction and it becomes about 7 times the freestream velocity because of gas expansion by the temperature increase.

Fine nanometer to micrometer particles are strongly affected by thermophoretic forces when placed in a steep temperature gradient [8][9][16][17]. Particles in the temperature gradient have a drift velocity towards the lower temperature direction almost proportional to the temperature gradient. In a sooting flame there is a steep temperature gradient and the soot particles formed in the flame are exposed to the temperature gradient.

The theory of thermophoresis of particles has substantially different forms depending on the value of the Knudsen number, Kn, [18]~[21]:

$$Kn = \lambda / R \qquad (1)$$

Where λ is the mean free path and R is the radius of the particles.

There is no formula to cover all Kn values for the calculation of the thermophoretic force. Therefore, depending on the Kn or particle size, a careful choice of formula to calculate the thermophoretic force is important. When $\lambda/R \gg 1$, the regime is called the free-molecular regime. In this regime particles are very small and the molecular mean free path is large. For $0.01 < \lambda/R < 1$ the regime is called the slip-flow regime.

As soot agglomerates can be fairly large, more than 10 microns as shown in previous work[22][23],

it would be reasonable to use the formula for the slip-flow regime, as proposed by Brock[18] and Derjaguin[19]. However, Dobashi et al. reported that the thermophoretic velocities evaluated by the two equations are much smaller than the values measured in their experiments [24][25] independent of agglomeration size. They also showed that soot agglomerates under thermophoretic forces behave as individual fine primary particles in the free-molecular regime rather than as large size particles in the slip-flow regime. The reason for this behavior must lie in the soot agglomerate structure, with fine primary particles of high void ratios. Therefore, the formula suitable for the free-molecular regime proposed by Waldmann [20][21] was selected to estimate the thermophoretic effect here, even when the apparent soot agglomerate size gives Knudsen numbers much smaller than unity. The Waldmann formula used to estimate the drift velocity caused by the thermophoretic effect is:

$$U_t = -\frac{3\nu}{4(1+\frac{\pi}{8}\alpha_m)} \cdot \frac{\nabla T}{T} \qquad (2)$$

where, ν is the kinetic viscosity, ∇T is the temperature gradient, T is the mean absolute temperature, and α_m is an accommodation coefficient(assumed to be unity)

Figure 10 shows the thermophoretic drift velocity, U_t; gas velocity, U_g; particle velocity, $U_p(=U_g+U_t)$; and the temperature distribution at z=90mm based on the calculations in Fig.9. The thermophoretic velocity U_t was calculated with formula (2). In Fig. 10, the gas velocities, U_g, very near the surface of the wall are near 0, and the particle velocity is almost exclusively determined by the thermophoretic velocity. This implies that the thermophoretic force is a dominant factor in the soot motion very near the surface of a wall. At T_a=600K, the temperature gradient is steeper than at T_a=300K meaning that soot more easily adheres to the wall here.

Figure 11 shows an outline of soot deposition on the wall at T_a=300K and 600K. It was assumed that already formed soot particles were present in the flow field. The velocity vectors in the figure indicate the particle motion at each point, $U_p(=U_g+U_t)$ in the r-direction and $V_p(=V_g+V_t)$ in the z-direction; the shading shows $U_p(=U_g+U_t)$ in the r-direction. The solid arrows in the figure show soot lines without

considering the thermophoretic velocity starting from the stagnation point in the r-direction where the velocity at the fuel exit and the velocity of the gas by heat expansion from the flame side balances. The dotted arrows in Fig.11 are soot lines including the thermophoretic velocity in addition to the gas convection motion. Without considering the thermophoretic velocity, the velocity of a particle should be the same as the velocity of the gas. Under this condition, it is difficult for soot to deposit on the wall at both temperature conditions (T_a=300K and 600K) because the normal velocity towards the wall becomes smaller at positions closer to the wall. Compared with the experimental result in Fig.6, it can be understood that the motion indicated by the solid arrow is different from the actual motion. When considering the thermophoretic velocity under the assumption of a free-molecular regime, the soot line approaches the direction of the surface of the wall at T_a=600K, and finally reaches the wall. However, in the T_a=300K case, the line did not reach the surface of a wall even with the thermophoretic velocity, although the position of the soot line migrates more towards the wall than the soot line without the thermophoretic effect. The reasons for the differences in the two cases are the differences in starting position and temperature gradients. In the high temperature case, a volumetric expansion of the approaching air causes a higher flow velocity, which moves the fuel distribution closer to the wall than in the low temperature case. The resulting flame position is closer to the wall as also shown in Fig.5 for the higher temperature case, and this results in a closer position of stagnation of the fuel injection and gas expansion motions in the z-direction and the steep temperature gradient between flame and wall. The calculated results here are in good agreement with the experimental results, and demonstrate that a consideration of the thermophoretic effect is essential to estimate soot deposition phenomenon and that the assumption of a free molecular regime is a reasonable one in evaluating the effect on soot particles in flames in microgravity experiments. The calculated results here are the first data simulating soot distribution in a flame burning along a solid wall. These results would make a considerable contribution to an optimization of the design of high temperature combustion systems such as boiler furnaces with heat exchangers and the reaction tubes of steam reformers, which often suffer from problems with soot deposition on the heat exchangers.

5. Conclusions

The effect of the surrounding air temperature on soot particle behavior under laminar diffusion flames formed along a solid wall was investigated to provide basic information of actual soot deposition in heat exchangers in high temperature combustion systems. The results may be summarized as follows:

1. Using a microgravity environment, the in-situ soot adhesion process to walls in a boundary layer like diffusion flame along a solid wall was obtained by attaining a stable buoyancy-free flame, a first in the literature. According to the observations, the soot volume fraction increases and the distribution moves closer to the wall with increases in the surrounding air temperature, and the resulting amount of soot deposition on the wall increases.

2. A comparison of the numerical calculations and experimental results shows that the soot adheres to the wall due to the thermophoretic effect; while there is no soot deposition on the wall when the thermophoretic effect is not considered. This indicates that a consideration of thermophoresis is essential to determine the behavior of soot deposition in flames.

3. By applying the Waldmann formula for the free-molecular regime, the calculated results are in good agreement with the observed soot behavior in a laminar diffusion flame along a solid wall under microgravity. This shows that the assumption of the free molecular regime is a reasonable one when evaluating the thermophoretic effect on soot particles present in flames in the microgravity experiments.

Acknowledgement

This work was supported by the NEDO (New Energy Development Organization of Japan) through the JSUP (Japan Space Utilization Promotion Center) and ECCJ (Energy Conservation Center,

Japan) as a part of the R&D project on High Temperature Combustion Technology.

References

(1) Athanasios, G., Konstandopoulos., and Rosner, D. E., Inertial Effects on Thermophoretic Transport of Small Particles to Walls with Streamwise Curvature, Int. J. Heat Mass Transfer 38 (1995), p. 2317-2232

(2) Walker, K. L., Homsy, G, H., and Geyling, F. T., Thermophoretic Deposition of Small Particles in Laminar Tube Flow, J. Colloid Interface Sci. 69 (1979), p.138-147

(3) Adomeit, P., Renz, U., Deposition of Fine Particles from a Turbulent Liquid Flow:Experiments and Numerical Predictions, Chemical Engineering Science. Vol.51, No.13 (1996), p.3491-3503

(4) Thakurta, D. G., Chen, M., Mclaughlin, J. B., and Kontomaris, K., Thermophoretic Deposition of Samll Particles in a Direct Numeriacal Simulation of turbulent Channel Flow, Int. J. Heat and Mass transfer 41 (1998), p.4167-4182

(5) Tsai, R., Liang, L. J., Correlation for Thermophoretic Deposition of Aerosol Particles onto Cold Plate, J. Aerosol Sci., 32 (2001), p.473-487

(6) Lin, J. S., Tsai, C.J., Thermophoretic Deposition Efficiency in a Cylindrical Tube taking into account Developing Flow at the Entrance Region, J. Aerosol Sci., 34 pp. 569-583 (2003).

(7) Dobashi, R., Kong, Z. W., Toda, A., Takahashi, N., Suzuki, M., and Hirano, T., Mechanism of Smoke Generation in a Flickering Pool Fire, Proc.of 6th Fire Safety Science (1995), p.255-264

(8) Toda, A., Ohinishi, H., Dobashi, R., Hirano, T., and Sakuraya, T., Experimental Study on the between Thermophoresis and Size of Aerosol Particles, Int. J. Heat Mass Transfer 41 (1998), p.2710-2713

(9) Toda,A., Ohi,Y.,Dobashi,R.,Hirano,T., and Sakuraya,T., Accurate Measurement of Thermophoretic Effect in Microgravity, J. Chem. Phys, 105(16), (1996), p.7083-7087

(10) Pushkar. T., James P. T., Xiaodong. F., Amy. R., Estimation of Particle Volume Fraction, Mass fraction and Number density in Thermophoretic deposition systems, J. Heat and Mass Transfer 46 (2003), p.3201-3209

(11) Joanne M. S., Alan. W., and Douglas. H., Soot and carbon Deposition Mechanisms in ethane/air flames, Fuel Vol. 74 No. 12 (1995), p.1753-1761

(12) Mahalingam, S., Cantwell, B. J., and Ferziger, J. H., Non-premixed Combustion: Full Numerical Simulation of a Coflowing axisymmetric Jet, Inviscid and Viscous Stability Anaysisi, report TF-43, Thermoscience Division, Stanford University, Stanford, California, (1989)

(13) Najm, H. N., Wyckoff, P. S., and Kino, O. M., J. Comput. Phys. 143 (1998), p.381-402

(14) Kee, R. J., Rupley, F. M., Meeks, E., and Miller, J. A., *CHEMKIN-III: A FORTRAN Chemical Kinetics Package for the Analysis of Gas-Phase Chemical and Plasma Kinetics*, SAND96-8216, Sandia National Laboratories, Livermore, CA, 1996.

(15) Kee, R. J., Warnatz, J., and Miller, J. A., A FORTRAN Computer Code Pakage for the Evaluation of Gas Phase Viscosities, Conductivities and Diffusion Coefficients, Sandia report SAND83-8209.

(16) Rosner, D.E., Mackowski, D.W. and Garcia-Ybarra, P., Size- and Structure- Insensitivity of the Thermophoretic of Aggregated Soot Particles in Gases, Combustion Science and technology, 80, (1991), p.87-101

(17) Fujita, O., and Ito, K., Observation of Soot agglomeration Process with Aid of Thermophoretic force in a Microgravity jet Diffusion Flame, J Experimental Thermal and Fluid Science, Elesevier Science, vol.26, Issues 2-4 (2002), p.305-311

(18) Brock, J.R., On the Two Theory of Thermal Forces Acting on Aerosol Particles, J. Colloid Sci, (1962), p.768-780

(19) Derjaguin,B.V. and Yalamov,Y., Theory of Thermophoresis of large Aerosol Particles, J.Colloid Sci.,20, (1965), p.555-570

(20) Waldmann, L., Uber die Kraft eines Inhomogenen Gases auf Kleine Suspendierte Kugeln, Z.Naturforschung,14a, (1959), p.589-599

(21) Waldmann., On the Motion of Spherical Particles in Nonhomogeneous gases, Academic Press Inc., (1961), p.323-344

(22) Ito, H. Fujita, O., Ito, K., Agglomeration of Soot Particles in diffusion Flames under Microgravity, Combust. Flame, 99 (1994), p.363-370

(23) Fujita,O., Takeshita,Y., Effect of Thermophoretic Force on Soot Agglomeration Process in Diffusion

Flames under Microgravity, The Fourth International Microgravity Combustion Workshop (NASA CP-1997-10194) (1997), p.217-222

(24) Ono, H., Dobsashi,R., Sakuraya,T., Effect of Thermophoresis on Soot Particles, Proc.of 39th Japanese Combustion Symposium (in Japanese) (2001), p.129-130

(25) Ono, H., Dobashi,R., Sakuraya,T., Thermophoretic Velocity Measurement of soot Particles under a Microgravity condition, Proc. Combustion Institute Vol.29 (2002), p.2375-2382

FIGURE CAPTIONS

Fig.1 **A Schematic outline of the cylindrical burner**

Fig.2 **A Schematic outline of the experimental setup**

Fig.3 **Laminar diffusion flames in normal gravity and micrograity (Fuel C_2H_4, U_f=0.8cm/s, V_a=5cm/s, O_2=35%, N_2 balance, T_w=300K)**

Fig.4 **Direct image and Extinction image stabilized around the cylindrical burner with surrounding air temperature of 300 and 600K (Fuel C_2H_4, U_f=0.8cm /s, V_a=5cm/s, O_2=35%, N_2 balance, T_w=800K)**

Fig.5 **Maximum soot concentration position (soot line) and visible flame position (flame line) along the flow direction for different air temperatures (Fuel C_2H_4, U_f=0.8cm /s, V_a=5cm/s, O_2=35%, N_2 balance, T_w=800K)**

Fig.6 **Actual soot deposition with different air temperatures (Fuel C_2H_4, U_f=0.8cm /s, V_a=5cm/s, O_2=35%, N_2 balance, T_w=800K)**

Fig.7 **Soot volume fraction distributions normal to the flow direction at different z position(Fuel C_2H_4, U_f=0.8cm/s, V_a=5cm/s, O_2=35%, N_2balance, T_w=800K)**

Fig.8 **Physical model of soot particle motion under the effect of flow and thermophoretic forces**

Fig.9 **Temperature and velocity distributions obtained by numerical calculations (O_2=35%,T_w=800K)**

Fig.10 **Thermophoretic velocities, U_t; gas velocities, U_g; particle velocities, U_p; and temperature distributions at z=90mm(O_2=35%,T_w=800K)**

Fig.11 **Particle motion vectors (U_p+V_p), particle velocity contours (shading, U_p), soot lines considering the thermophoretic velocity (dotted arrow) and soot lines without the thermophoretic velocity (solid arrow) (O_2=35%,T_w=800K)**

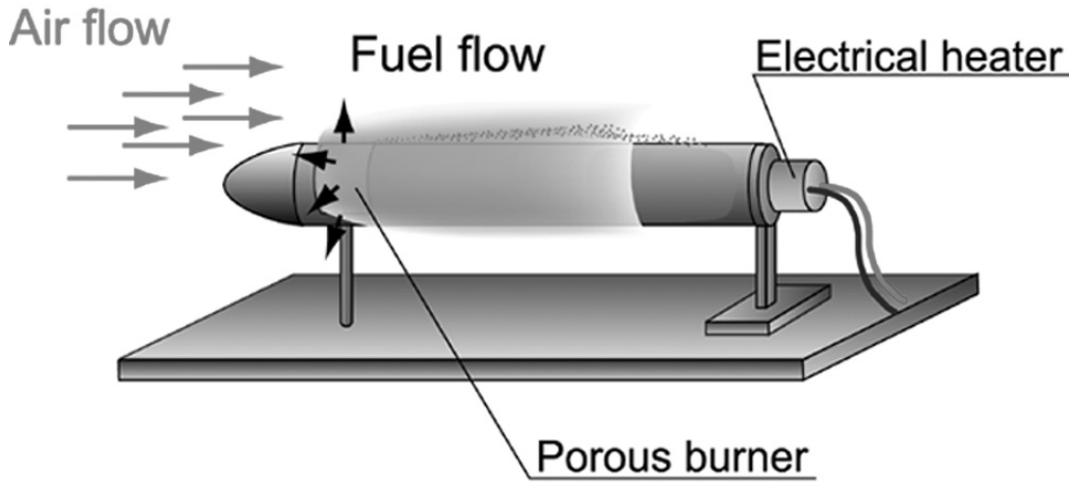

Fig.1 A Schematic outline of the cylindrical burner

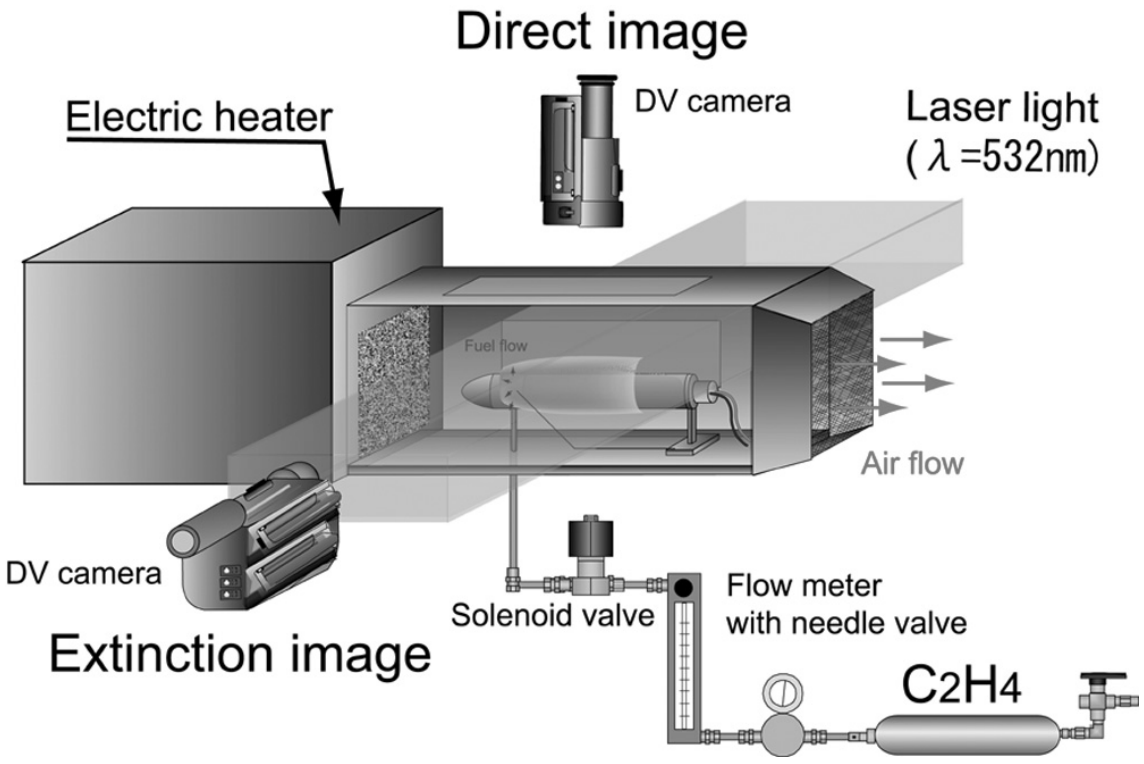

Fig.2 A Schematic outline of the experimental setup

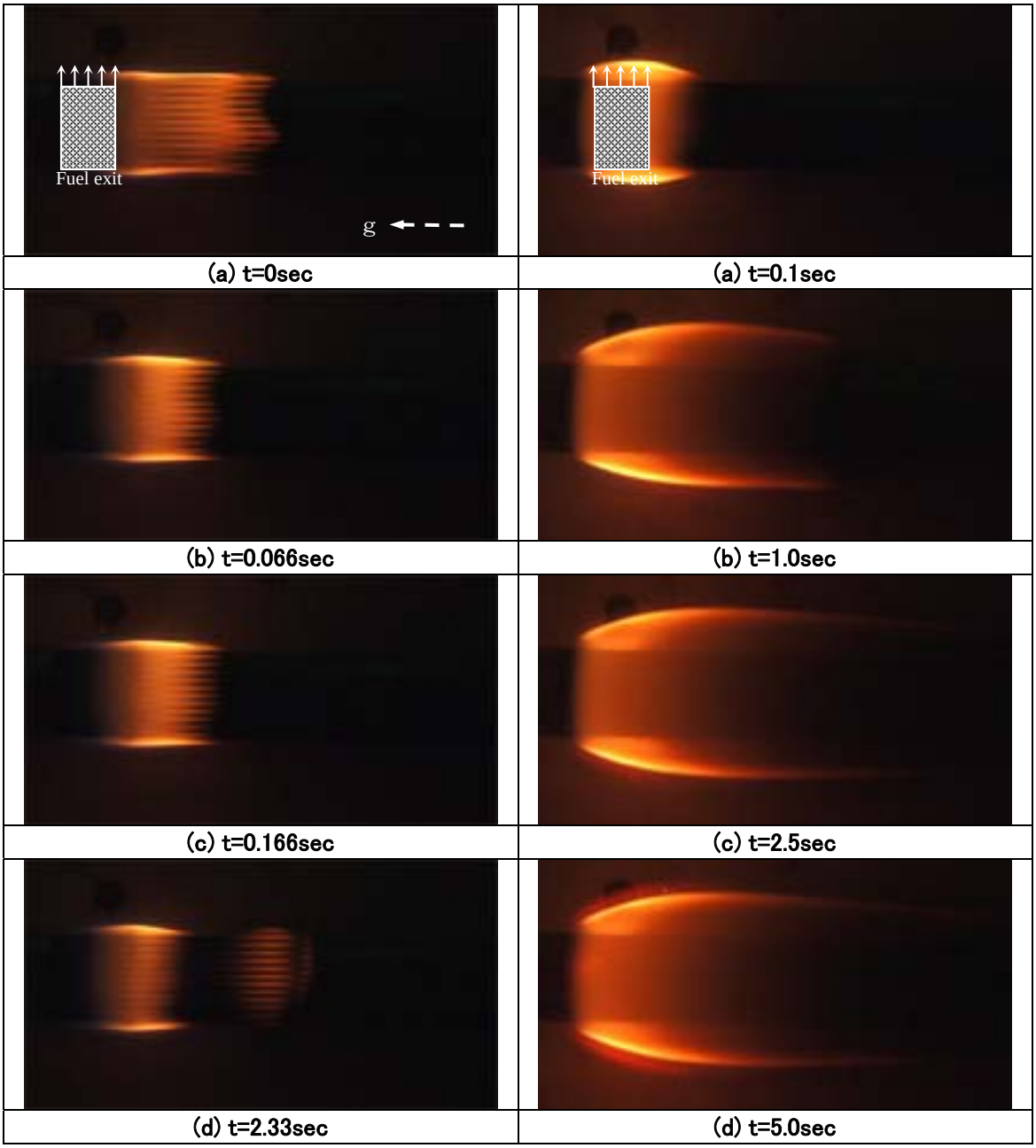

Fig.3 Laminar diffusion flames in normal gravity and micrograity

(Fuel C_2H_4, U_f=0.8cm/s, V_a=5cm/s, O_2=35%, N_2 balance, T_w=300K)

(a) T_a=300K

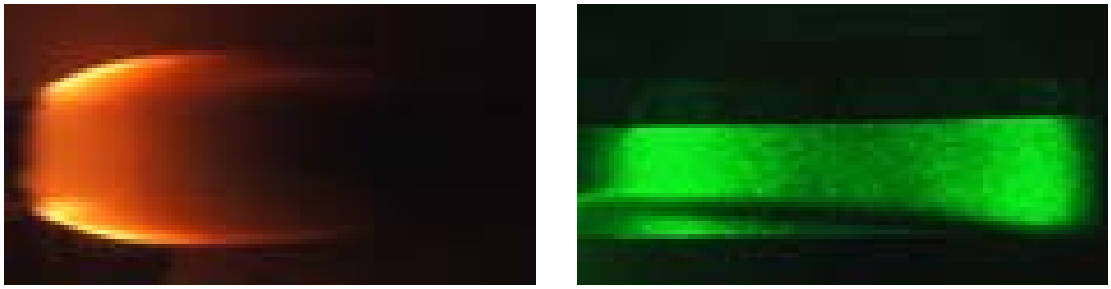

(b) T_a=600K

Fig.4 Direct image and Extinction image stabilized around the cylindrical burner with surrounding air temperature of 300 and 600K (Fuel C_2H_4, U_f=0.8cm/s, V_a=5cm/s, O_2=35%, N_2 balance, T_w=800K)

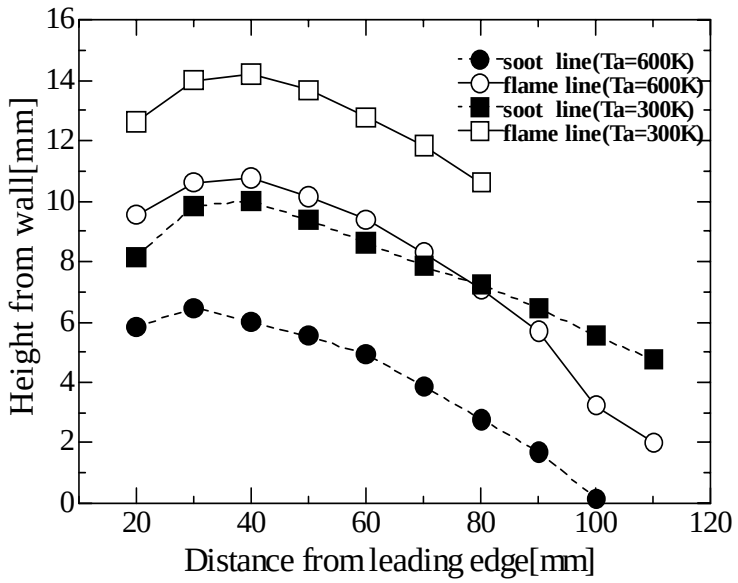

Fig.5 Maximum soot concentration position (soot line) and visible flame position (flame line) along the flow direction for different surrounding air temperatures (Fuel C_2H_4, U_f=0.8cm/s, V_a=5cm/s, O_2=35%, N_2 balance, T_w=800K)

(a) T_a=300K

(b) T_a=600K

Fig.6 Actual soot deposition with different air temperatures

(Fuel C_2H_4, U_f=0.8cm/s, V_a=5cm/s, O_2=35%, N_2 balance, T_w=800K)

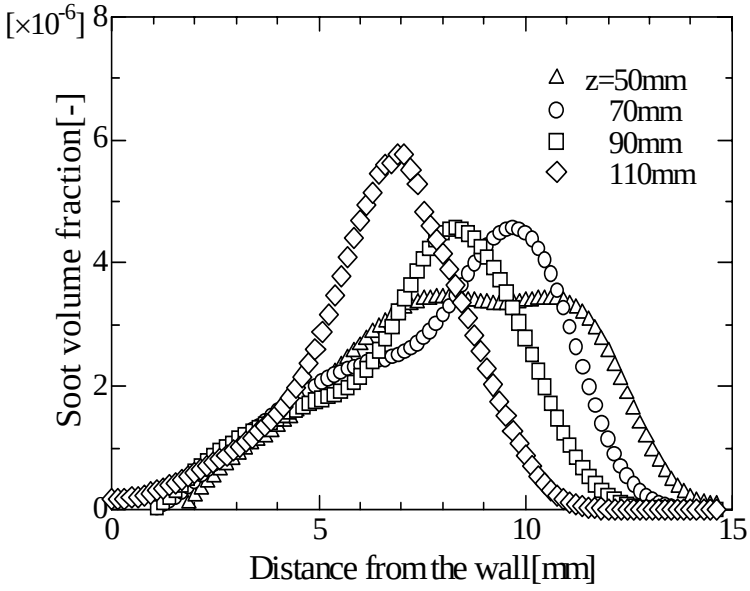

(a) T_a=300K

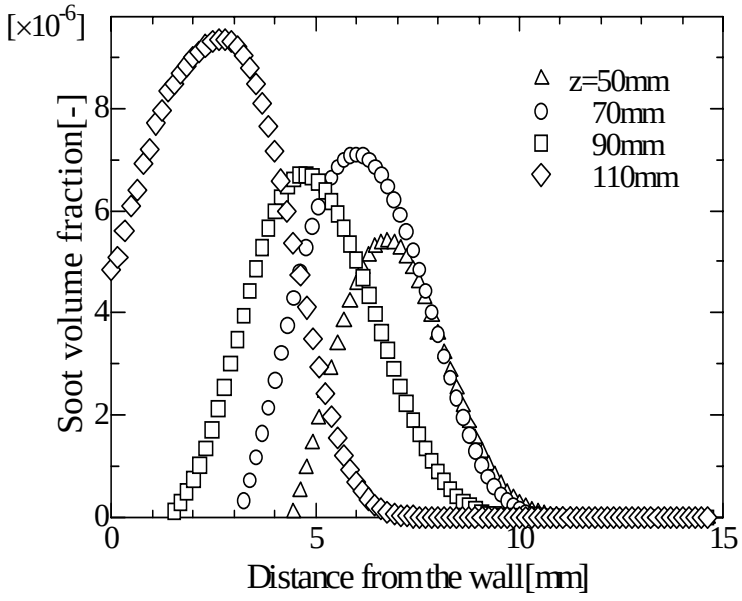

(b) T_a=600K

Fig.7 Soot volume fraction distribution normal to flow direction at different z position (Fuel C_2H_4, U_f=0.8cm/s, V_a=5cm/s, O_2=35%, N_2 balance, T_w=800K)

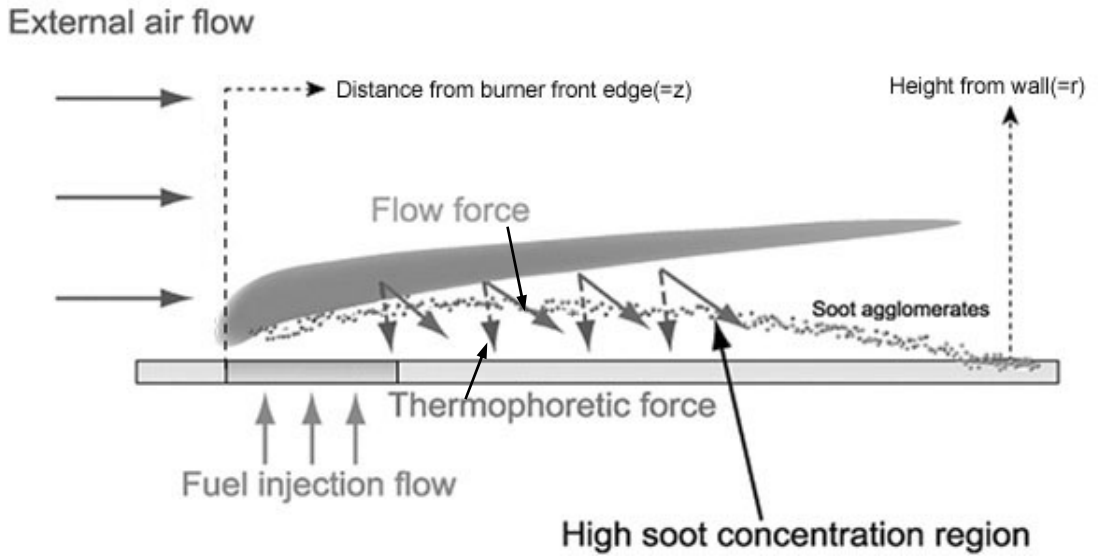

Fig.8 Physical model of soot particle motion under the effect of flow force and thermophoretic forces

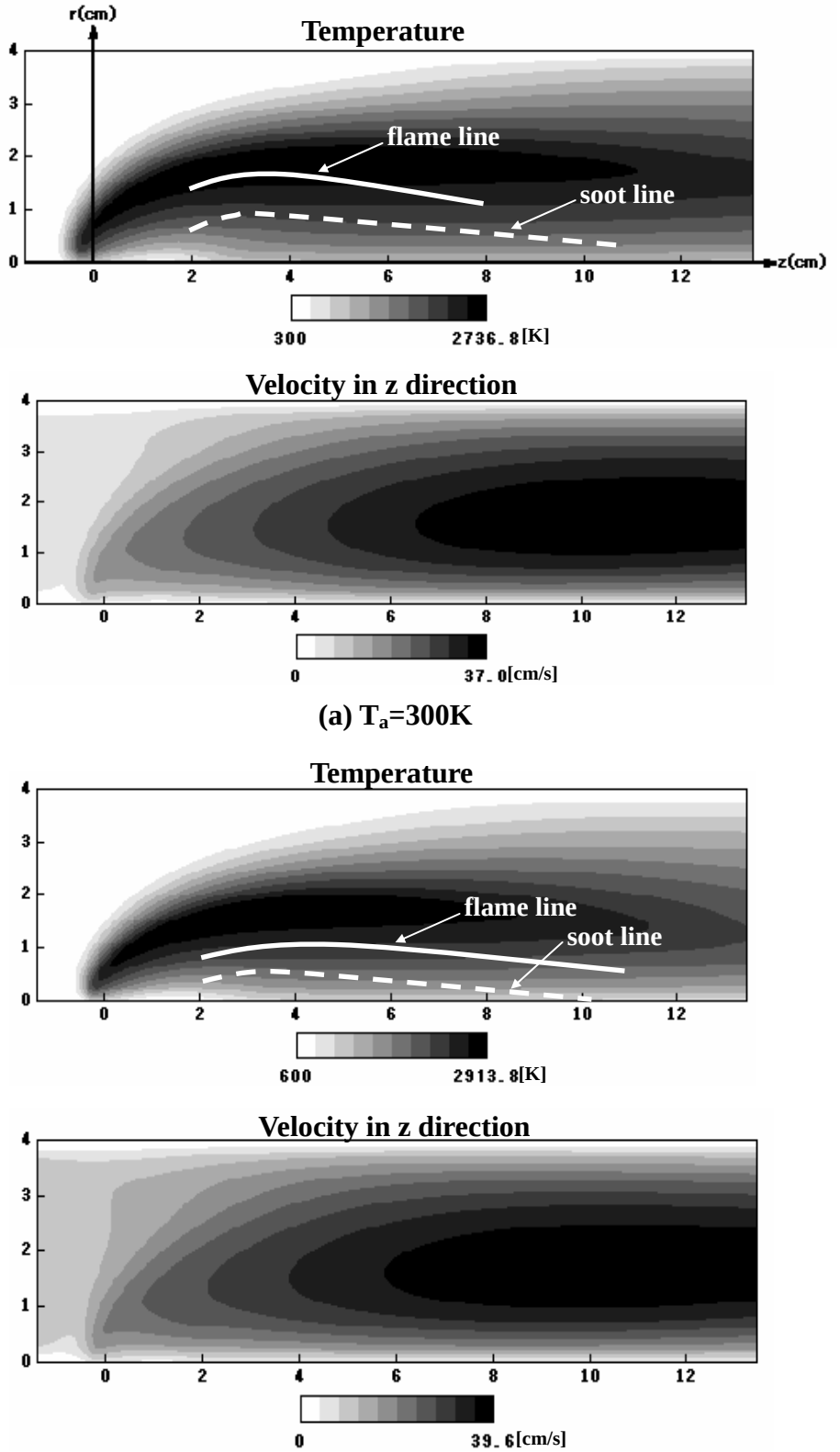

(a) T_a=300K

(b) T_a=600K

Fig.9 Temperature and velocity distributions obtained by numerical calculation

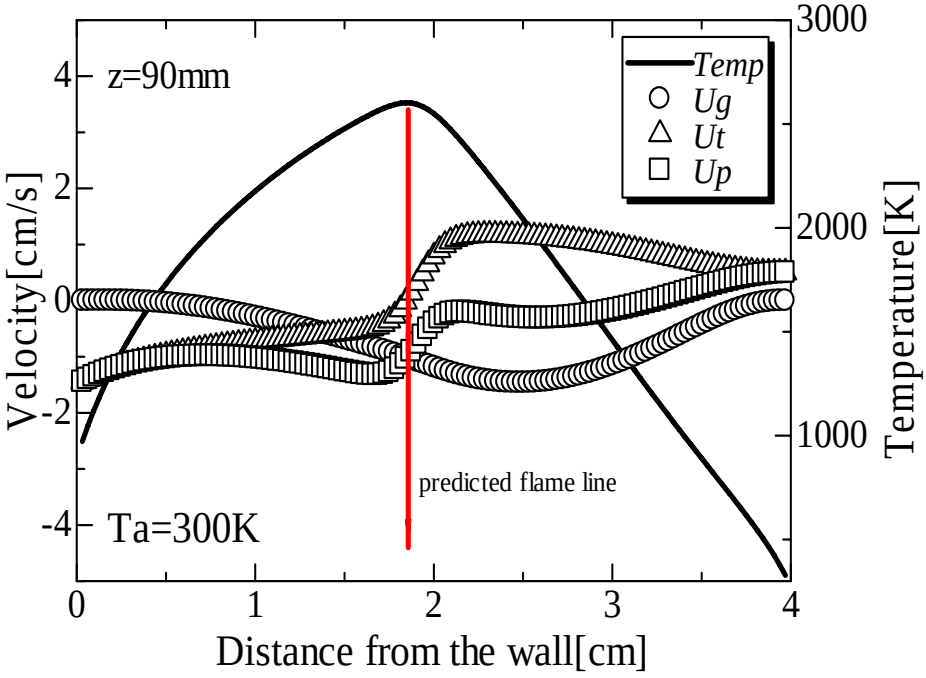

(a) T_a=300K

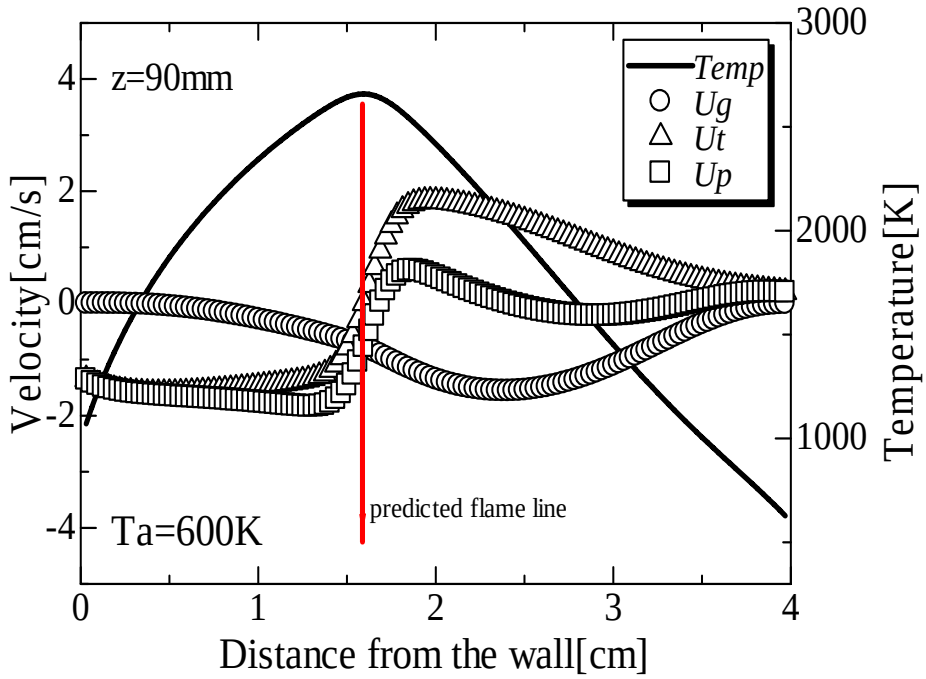

(b) T_a=600K

Fig.10 Thermophoretic velocities, U_t; gas velocity, U_g; particle velocities, U_p; and temperature distributions at z=90mm (O_2=35%,T_w=800K)

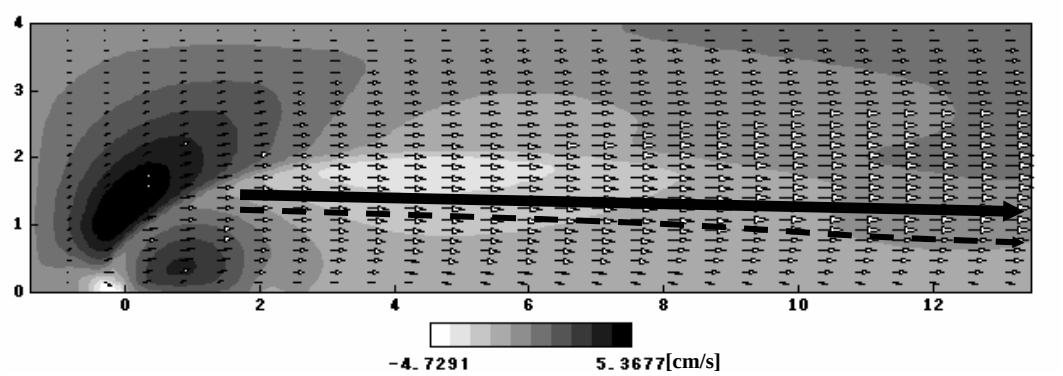

(a) T_a=300K

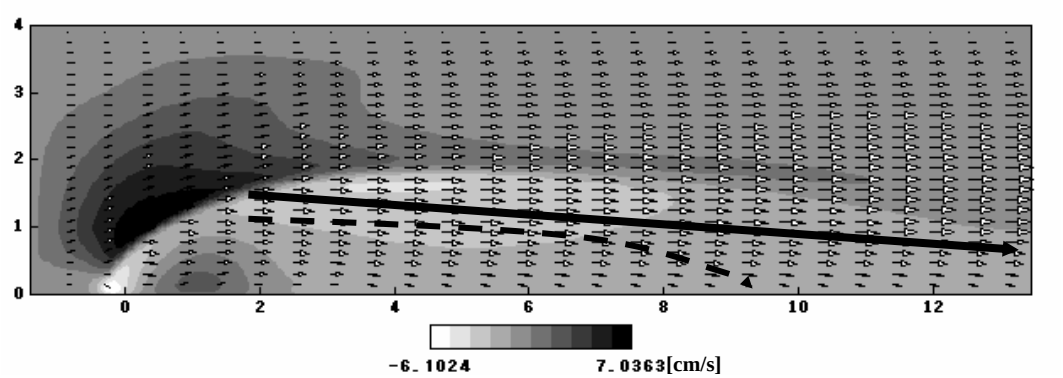

(b) T_a=600K

Fig.11 Particle motion vectors (U_p+V_p), particle velocity contours (shading, U_p), soot lines considering the thermophoretic velocity (dotted arrow) and soot lines without the thermophoretic velocity (solid arrow) (O_2=35%,T_w=800K)